ACS Photonics

Letter

pubs.acs.org/journal/apchd5

Strong Local Chiroptical Response in Racemic Patchy Silver Films: Enabling a Large-Area Chiroptical Device

Yizhuo He,* Keelan Lawrence, Whitney Ingram, and Yiping Zhao

Department of Physics and Astronomy, and Nanoscale Science and Engineering Center, University of Georgia, Athens, Georgia 30602, United States

Supporting Information

ABSTRACT: Ag glancing angle depositions on polycrystalline colloid monolayers can produce a variety of chiral or achiral Ag nanostructures in different colloid monolayer domains, whose geometric shapes strongly depend on the monolayer orientations. The morphological and chiroptical properties of these Ag nanostructures in different colloid monolayer domains are investigated both experimentally and theoretically, and their relationship has been revealed. Extremely strong local circular dichroism is observed for the domains with obviously chiral morphologies. Under the guidance of this individual domain study, large-area chiral metamaterials can be fabricated on the monocrystalline monolayers with strong, uniform, and tunable chiroptical response, which can be potentially developed into optical devices.

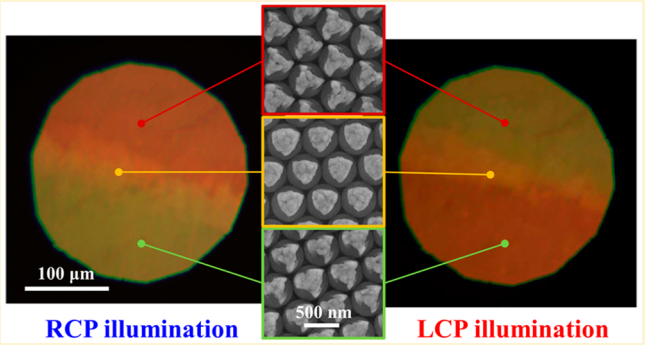

KEYWORDS: *glancing angle deposition, chiral metamaterial, plasmonics, circular dichroism, patchy particles*

The past decade has witnessed a rapid development of chiral metamaterial, an important branch of metamaterials.[1] Chiral metamaterials are artificial structures that cannot be superposed with their mirror images. Their structural chirality often leads to different interactions with left-handed circularly polarized (LCP) and right-handed circularly polarized (RCP) light, such as a rotating polarization plane of light, known as optical rotation, and different absorbance for LCP and RCP light, known as circular dichroism (CD). These chiroptical effects also exist in natural molecules, but are orders of magnitude weaker than those of artificially designed chiral metamaterials.[2] With the advance of mirco/nanofabrication technology, a variety of chiral metamaterials have been realized,[3−13] enabling applications in negative refraction,[14,15] light polarization manipulation,[3,16−18] controlled CD switching,[19−22] second-harmonic generation,[23−25] superchiral field based biosensing,[26] etc.

Recently, based on self-assembled colloid monolayers (SACMs), glancing angle deposition (GLAD) has been demonstrated as a powerful and scalable fabrication technique for chiral metamaterials.[27−30] GLAD is a physical vapor deposition technique that relies on the geometric shadowing effect to create nanostructures. SACMs serve as deposition templates for GLAD to produce two-dimensional regular patterns of nanostructures. Since SACMs are usually polycrystalline, GLAD on SACMs produces so-called "patchy particles", which are particles within designated regions or "patches" of specific properties that are different from the rest of the particles. The morphology of the patchy particles is directly determined by the polar and azimuthal orientation of the monolayer domains with respect to the direction of the incident vapor flux. Therefore, a GLAD process will result in patchy films with different morphologies in differently orientated domains. In our previous study, we fabricated Ag patchy films on polycrystalline monolayers with randomly orientated domains, which leads to an equal portion of morphological enantiomers.[27] Such a racemic mixture was not expected to show chiroptical response. However, the investigation of bulk CD response indicated that the racemic symmetry is broken by the difference in material accumulation on the monolayer beads affected by the substrate rotation direction during GLAD, resulting in an incomplete cancellation of strong local chiroptical response. The CD response of individual domains was visualized by the microscope images taken under circularly polarized light and was also estimated to be an order of magnitude larger than bulk CD over wavelengths of 700−800 nm. However, accurate CD measurements of individual domains have not been performed and are greatly needed. The relationship between CD response and morphology of patchy films has not been clearly understood. In this study, we investigate both the morphological and optical properties of different domains of Ag patchy films. We demonstrate that these Ag patchy particles contain a variety of achiral and chiral nanostructures with their CD responses strongly depending on their morphologies. Both experiments and simulations confirm that some particularly orientated domains can exhibit a giant CD response, which is an order of magnitude larger than the bulk CD response and agrees with our previous estimation. On the

Received: April 13, 2015
Published: August 20, 2015

DOI: 10.1021/acsphotonics.5b00196
ACS Photonics 2015, 2, 1246−1252

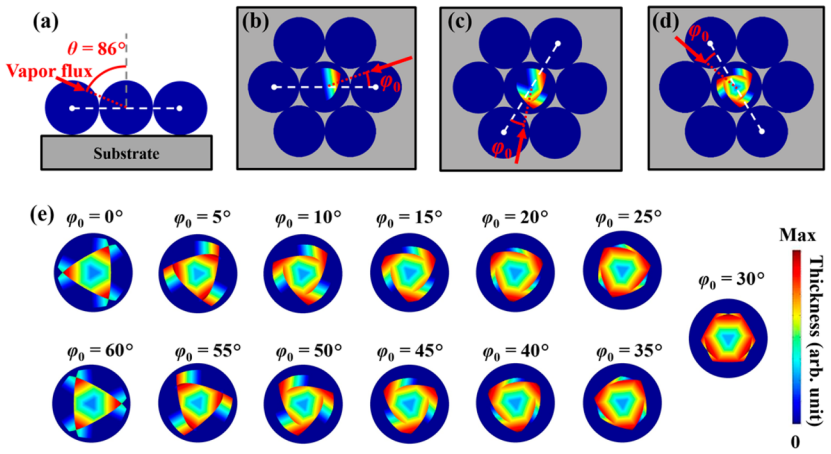

Figure 1. Scheme of fabrication process of Ag patchy films and morphology simulations. (a) Ag vapor flux is incident upon the monolayer at an oblique angle $\theta = 86°$ with respect to the substrate normal. (b–d) Ag vapor flux is incident upon the monolayer in three azimuthal directions with an interval of $\Delta\varphi = 120°$. The azimuthal direction of Ag vapor flux and a dashed line going through the centers of the nanospheres form an angle, φ_0. (e) Simulated morphologies of Ag patchy films in differently orientated domains with $\varphi_0 = 0°$, 5°, 10°, 15°, 20°, 25°, 30°, 35°, 40°, 45°, 50°, 55°, and 60°.

basis of this individual domain study, Ag chiral films have been fabricated on a cm^2-size monocrystalline monolayer and show giant CD response, which can be used for future device applications.

The fabrication process for the Ag patchy films has been described in our previous work[27] and is briefly summarized here. First, a hexagonal close-packed (HCP) monolayer of polystyrene nanospheres with diameter $D = 500$ nm was created as a deposition template. The monolayer had polycrystalline domains with areas of 0.0001–1 mm^2. Then Ag vapor was deposited onto the monolayer at a polar angle $\theta = 86°$ with respect to the substrate normal, as shown in Figure 1a. After a 30 nm Ag deposition, the substrate was azimuthally rotated by $\Delta\varphi = 120°$, and then another Ag layer of 30 nm was deposited. This process was repeated until a total nominal film thickness of 360 nm and a total substrate rotation of $4 \times 360°$ were achieved. The azimuthal angle of incident vapor for each monolayer domain φ_0 can be defined as the relative angle of vapor flux direction with respect to a virtual straight line through the centers of nanospheres, which is chosen properly to ensure $0° \leq \varphi_0 < 60°$ due to the 6-fold rotational symmetry of the HCP lattice of the monolayer, as shown in Figure 1b–d. The monolayer domains in the same orientation have the same φ_0, and the differently orientated domains have different φ_0. In other words, φ_0 can be used to define the orientation of each domain. Note that in the previous work the substrate can be rotated azimuthally clockwise or counterclockwise during depositions to produce films with opposite bulk CD responses. In this work, we investigate only the individual domains on the samples rotated counterclockwise.

The morphology of patchy films can be estimated by a simple morphology simulation, which considers only the shadowing effect of adjacent nanospheres. The details of the morphology simulation can be found in the Supporting Information of our previous work.[27] Figure 1e shows the simulated morphologies of the Ag films on monolayer domains with different φ_0. It is found that the Ag films with azimuthal angles of φ_0 and $60° - \varphi_0$ are morphological enantiomers if the shadowing effect of deposited films is ignored. With $\varphi_0 = 0°$, the film has an achiral shape. As φ_0 increases, a chiral fan-shaped structure with three rotating arms is created. The arms of fan-shaped structures gradually become shorter and wider, and the structure finally becomes achiral as φ_0 approaches 30°.

Ag films on six representative domains (domains 1–6) are selected for both morphological and optical studies, and their top-view scanning electron microscope (SEM) images are shown in Figure 2a. Domains 1–6 have $\varphi_0 = 58°$, 3°, 52°, 9°, 23°, and 30°, respectively (see Supporting Information Section S1 for determining φ_0). As predicted by the morphology simulations, chiral fan-shaped structures are produced on domains 1–4 with φ_0 close to 0° or 60°, and achiral triangular and hexagonal structures are created on domains 5 and 6 with φ_0 close to 30°, respectively. Particularly, domains 1–2 and 3–4 form two pairs of morphological enantiomers, since the sum of their φ_0 is roughly equal to 60°. To characterize the dimensions of Ag nanostructures on different domains, a characteristic length l is defined as the distance from one vertex to the opposite edge or vertex of the triangular-shaped fans, triangles, or hexagons, as shown by the solid red lines in Figure 2a. l is measured for each domain and listed in Table 1. For domains 1–4, l is approximately equal to the arm length, and it is found that the arm length of domains 1 and 2 is larger than that of domains 3 and 4, which agrees with the morphology simulations. The SEM images were also taken at a tilt angle of 45° with respect to the substrate normal (see Supporting Information Section S2). These SEM images clearly show that the Ag chiral films on beads are three-dimensional chiral metamaterials.

The chiroptical response of individual domains can be visualized and measured by a custom spectroscopic microscope system with circularly polarized incident light (see Supporting Information Section S2 for details of the custom spectroscopic microscope system). Figure 2b shows the optical micrographs of domains 1–6 under LCP light illumination (left-side figure) and RCP light illumination (right-side figure). For each domain, the micrographs under LCP and RCP light illuminations were taken in the same region, and their color difference represents the chiroptical response. Domain 1 (domain 2) appears orange under LCP (RCP) light and red under RCP (LCP) light. Domain 3 (domain 4) appears green under LCP (RCP) light and red under RCP (LCP) light. For the morphological enantiomers, domains 1 and 2 or domains 3 and 4, their colors are interchanged when switching the circular polarizations, indicating opposite chiroptical responses. Domain 5 shows an orange color and domain 6 shows a red color under both LCP and RCP light. No distinct color

DOI: 10.1021/acsphotonics.5b00196
ACS Photonics 2015, 2, 1246–1252

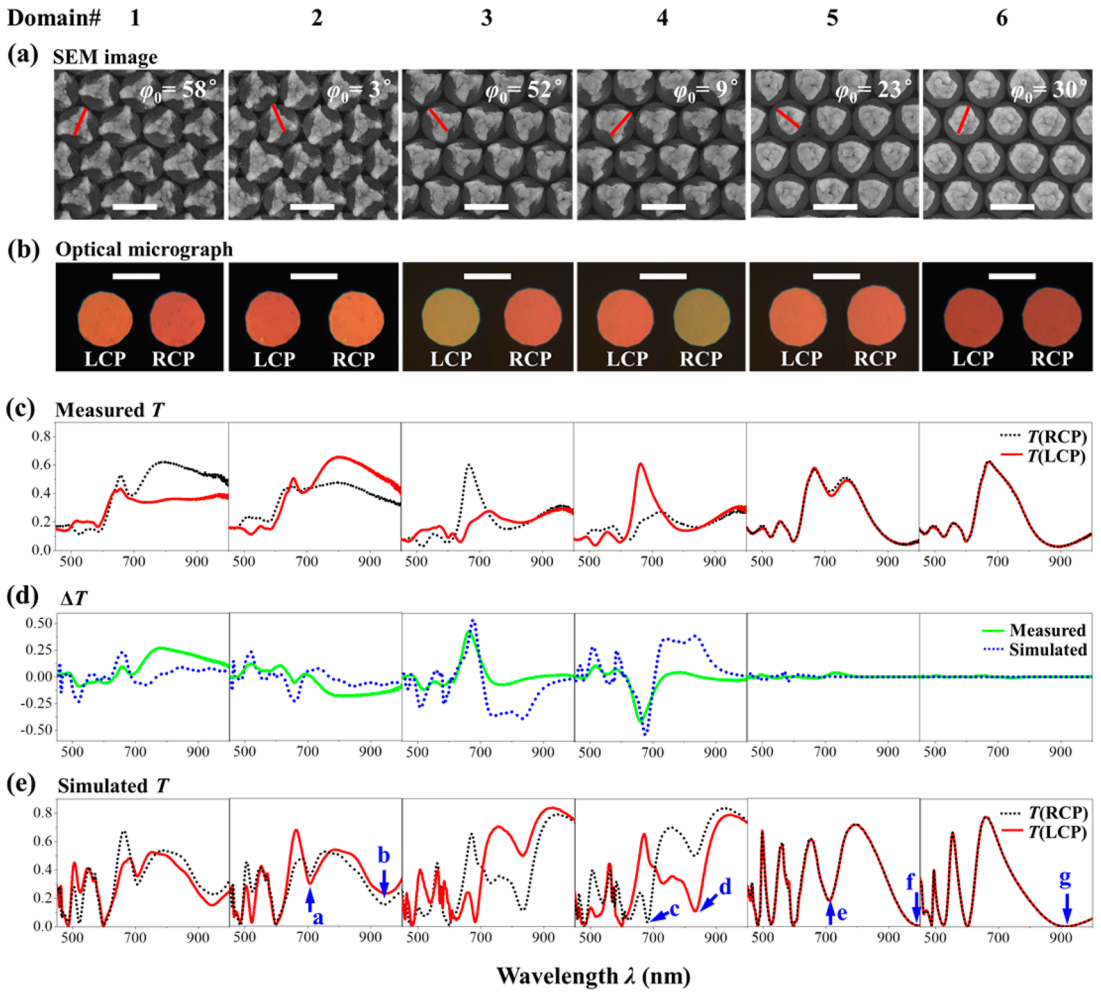

Figure 2. (a) SEM images, (b) optical micrographs under LCP and RCP light illuminations, (c) measured circularly polarized transmittance, (d) both measured and simulated differential circularly polarized transmittance ΔT, and (e) simulated circularly polarized transmittance, for domains 1−6. The scale bars in (a) and (b) represent 500 nm and 100 μm, respectively.

Table 1. Characteristic Length l of Ag Patchy Films for Different Domains

	domain no.					
	1	2	3	4	5	6
l (nm)	330 ± 30	330 ± 30	300 ± 40	310 ± 30	280 ± 20	380 ± 20

change between their LCP and RCP micrographs indicates weak or no chiroptical response, which is due to their achiral structures.

The circularly polarized transmittance spectra of domains 1−6, T(RCP) and T(LCP), were measured by the custom spectroscopic microscope system with circularly polarized incident light at normal incidence. Differential circularly polarized transmittance, $\Delta T = T(\mathrm{RCP}) - T(\mathrm{LCP})$, is used to characterize the CD response of the Ag patchy films. In order to minimize the contribution of polarization conversion to the circular polarization measurements, the transmittance spectra were measured in both front and back illumination modes and then averaged (see Supporting Information Section S3).[5] Figure 2c shows the measured T(RCP) and T(LCP) for domains 1−6. The measured ΔT spectra after averaging the front and back illumination measurements are shown with green solid lines in Figure 2d. All the domains have low transmittance (~0.05−0.2) in the short-wavelength range λ = 450−600 nm. This is mainly caused by the high-order localized surface plasmon resonance (LSPR) of Ag nanostructures and the increased scattered light not being collected in the zero-order transmittance measurement.[31] It should be noted that a transmittance dip around λ = 600 nm in both T(RCP) and T(LCP) spectra for all the domains corresponds to the photonic band gap of the two-dimensional periodic monolayers, which is determined by the refractive index contrast and the lattice constant of the monolayers.[32] For domain 1, T(RCP) is lower than T(LCP) in the wavelength range λ = 500−600 nm, leading to negative ΔT. T(RCP) becomes greater than T(LCP) in the long-wavelength range λ = 600−1000 nm, leading to positive ΔT, which makes the sample surface appear more red under RCP light than LCP light in the microscope. Both T(RCP) and T(LCP) have small peaks around λ = 650 nm, which results in a small positive peak in the ΔT spectrum. T(RCP) has two dips, at λ = 525 and 690 nm, due to the LSPR of Ag films, and a broad peak at λ = 780 nm, resulting in a positive broad peak in the ΔT spectrum. For domain 2, T(RCP) and T(LCP) spectra are similar to T(LCP) and T(RCP) spectra of domain 1, respectively, indicating

DOI: 10.1021/acsphotonics.5b00196
ACS Photonics 2015, 2, 1246−1252

that domains 1 and 2 have opposite ΔT. For domain 3, T(RCP) is lower than T(LCP) in the wavelength range λ = 500−600 nm with negative ΔT, which makes domain 3 appear green under LCP light in the microscope. In the wavelength range λ = 600−730 nm, T(RCP) becomes greater than T(LCP) with positive ΔT, which makes domain 3 appear red under RCP light in the microscope. T(RCP) shows two dips, at λ = 520 and 785 nm, and T(LCP) also shows two dips, at λ = 640 and 835 nm, corresponding to the LSPR of Ag films. A sharp transmittance peak appears in T(RCP) at λ = 666 nm, resulting in a sharp ΔT peak. As expected, domain 4 has similar transmittance spectra to domain 3, but with T(RCP) and T(LCP) spectra interchanged. For domains 5 and 6, their T(RCP) and T(LCP) spectra almost overlap with each other, indicating ΔT to be almost 0. Domains 5 and 6 have the same transmittance dip at λ = 470 and 530 nm, but show different LSPR wavelengths in the long-wavelength range, due to their different structures. Domain 5 has two resonances, at λ = 720 and 950 nm, while domain 6 has a resonance at λ = 890 nm. The transmittance dip at λ = 720 nm makes domain 5 transmit less red light than domain 6, which explains their color difference in the microscope. The circularly polarized transmittance measurements confirm the opposite chiroptical response of domains 1 and 2 (3 and 4) and weak or no chiroptical response of domains 5 and 6, which is consistent with their morphological chirality and the observation under the microscope. In addition, two pairs of enantiomers, domains 1−2 and 3−4, exhibit different spectral features, which originates from the differences in the shape and size of their structures. Note that since the morphology of Ag patchy films strongly depends on φ_0, other domains with different φ_0 can have different structures and thus show different CD spectra from those of domains 1−6, which are not shown here. Furthermore, the local CD response of individual domains can be extremely large. The magnitude of ΔT can reach 0.27 for domains 1and 2 and even 0.43 for domains 3 and 4. ΔT is also converted to the ellipticity η (see Supporting Information Section S4), which has a maximum magnitude of 20°. Both ΔT and η of certain local domains are 1 order of magnitude larger than the statistically averaged CD response of differently orientated domains, which has ΔT = 0.02 and η = 2° at maximum, and also larger than those reported in most chiral metamaterial studies.[5,6,9,11,16]

The chiroptical properties were also simulated by the finite-difference time-domain (FDTD) method (see Supporting Information Section S5). The simulated T(RCP) and T(LCP) spectra for domains 1−6 are shown in Figure 2e, and the calculated ΔT spectra are shown with dotted blue lines in Figure 2d. The geometric models of Ag films in FDTD simulations were created based on the top-view SEM images and are shown in Figure S5 in the Supporting Information. In the simulations, it is assumed that all the Ag films are uniformly coated on nanospheres with a thickness of 100 nm and a smooth surface. The SEM images in Figure 2a show that the three arms of chiral fan-shaped Ag films have different lengths, which results from the substrate rotation during depositions. However, in the FDTD simulations, the lengths of the three arms of a fan-shaped Ag nanostructure are assumed to be the same. These simple models are meant to capture the essential features of the CD response of each structure, and we have ignored the spatial distribution of Ag thickness and the morphological variation shown in Figure 2a. As shown in Figure 2d and e, regardless that multiple assumptions are made on the simulated structures, the FDTD simulations still successfully reproduce the main features of experimental results. For domains 1−6, all the resonances in the measured transmittance and differential transmittance spectra are well reproduced in the simulated spectra at almost the same wavelength positions. However, there are still some small differences between the measured and simulated spectra, such as an extra resonance at λ = 943 nm in the simulated transmittance spectra of domains 1 and 2 and an extraordinarily high transmittance in the near-infrared region in the simulated spectra of domains 3 and 4. These deviations could result from a small difference in size, shape, or thickness between simulated and actual structures. The near-field FDTD simulations were also performed to reveal the nature of the plasmonic resonances under circularly polarized incident light. Figure 3 shows the simulated

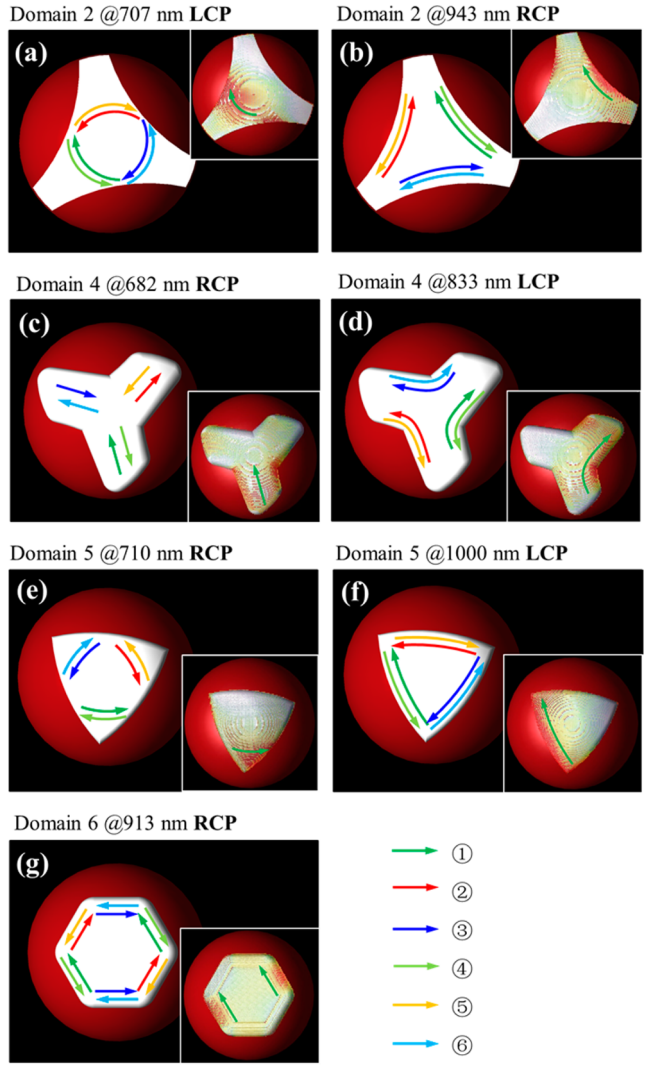

Figure 3. Simulated near-field current directions of (a) domain 2 with LCP incident light at λ = 707 nm, (b) domain 2 with RCP incident light at λ = 943 nm, (c) domain 4 with RCP incident light at λ = 682 nm, (d) domain 4 with LCP light at λ = 833 nm, (e) domain 5 with RCP incident light at λ = 710 nm, (f) domain 5 with LCP light at λ = 1000 nm, and (g) domain 6 with RCP incident light at λ = 913 nm. The insets are simulated current distributions when the currents are in the direction of the green arrows.

near-field current directions on Ag films from domains 2, 4, 5, and 6, at the plasmonic resonance wavelengths, which are labeled with blue arrows in Figure 2e. For simplicity, the near-field simulations of domains 1 and 3 are not shown here, because their current distributions will be the mirror images of those of domains 2 and 4, respectively. The arrows in different colors represent different

DOI: 10.1021/acsphotonics.5b00196
ACS Photonics 2015, 2, 1246−1252

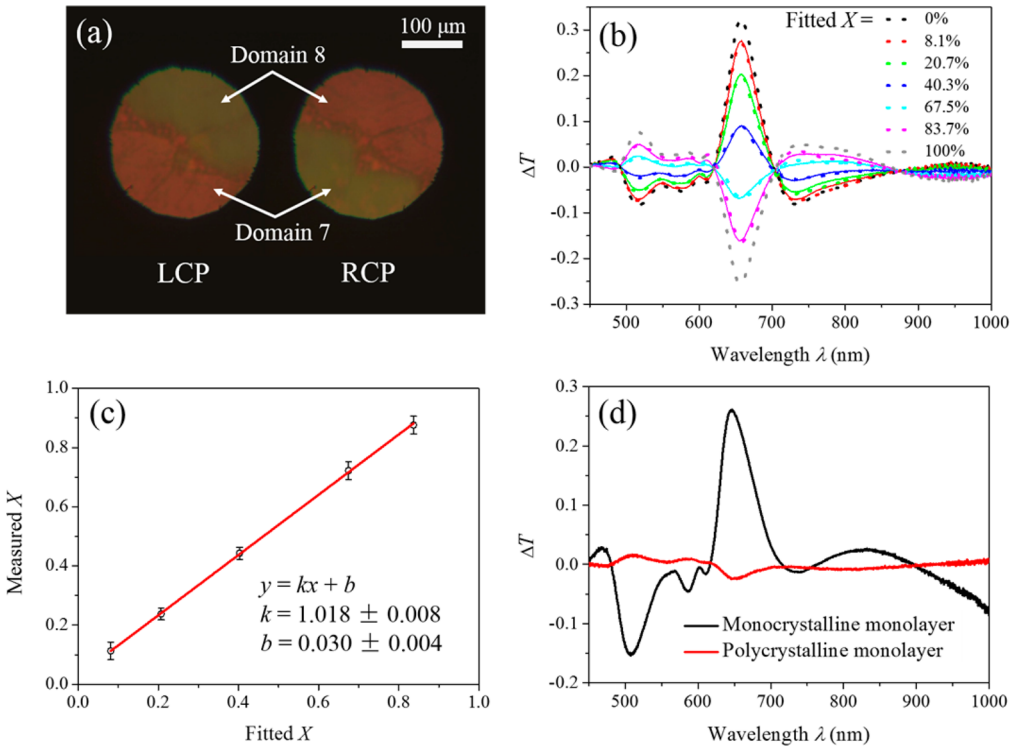

Figure 4. (a) Optical micrographs at a boundary of domains 7 and 8 under LCP and RCP illuminations. (b) Measured (dotted lines) and fitted (solid lines) ΔT spectra of a mixture of domains 7 and 8 with different area percentage X of domain 7. (c) Relationship between measured X and fitted X. (d) Bulk ΔT spectra of Ag films grown on both monocrystalline and polycrystalline monolayers.

plasmon oscillations, which have different phases and appear in the sequence as shown in Figure 3. The current distributions also exhibit 3-fold symmetry as the nanostructures. The insets in Figure 3 show the current distributions on the Ag film surfaces when the currents are in the directions of the green arrows.

The chiroptical measurements and simulations of individual domains reveal that the Ag patches with different φ_0 can exhibit different or even opposite CD responses. The polycrystalline nature of the monolayers allows the coexistence of Ag patches with opposite CD responses. These Ag patches on the same substrate can be individually examined by the spectroscopic microscope, which provides an excellent platform for the enantiomer sensing, benefiting from both their sharp CD peaks and the coexistence of patches with opposite CD responses.[26] When a mixture of these Ag patches is examined in a single CD measurement, their CD responses are supposed to be canceled out. In order to study how the Ag patches with opposite CD response contribute to the averaged CD signal, ΔT spectra of a mixture of two domains with opposite CD response were measured at their boundary by the spectroscopic microscope. The two domains are labeled as domains 7 and 8, as shown in the micrographs in Figure 4a. Domain 7 (8) appears red (green) under LCP illumination and green (red) under RCP illumination. ΔT spectra were measured with different area percentages of domain 7, X, and area percentages of domain 8, $1 - X$, which are shown by the dotted lines in Figure 4b (see Supporting Information Section S6, for more micrographs at different X). The spectra $\Delta T_{0\%}$ and $\Delta T_{100\%}$ are for the sampling area with only domains 8 and 7, showing similar spectral features to those of domains 3 and 4, respectively. The differential transmittance spectra $\Delta T(X)$ of the mixed domains are assumed to be a linear superposition of $\Delta T_{0\%}$ and $\Delta T_{100\%}$, i.e., $\Delta T(X) = (1 - X)\Delta T_{0\%} + X\Delta T_{100\%}$, which is used to fit the experimental spectra by the least-squares method to obtain the fitted X. The fitted spectra are shown by the solid lines in Figure 4b. X can also be measured directly in the micrographs and is plotted against the fitted X, as shown in Figure 4c. The relationship between measured X and fitted X is fitted by the linear function $y = kx + b$ with the slope $k = 1.018 \pm 0.008$ and the intercept $b = 0.030 \pm 0.004$, which indicates that the measured and fitted X are almost equal. This validates the linear superposition assumption and demonstrates that the contribution of a domain to the averaged CD signal is proportional to its area.

These Ag chiral metamaterials can be potentially developed into devices. For instance, domain 3 has a very sharp ΔT peak between $\lambda = 630$ nm and $\lambda = 720$ nm with a maximum value of $T(\mathrm{RCP})/T(\mathrm{LCP})$ greater than 5 (see Supporting Information Section S7), which may work as a band-pass filter for circular polarization. For the real device application, large-area substrates with uniform and high CD response are required. This can be realized by fabricating the fan-shaped Ag chiral nanostructures as those in domain 3 on the large-area monocrystalline monolayer templates. We fabricated the monocrystalline monolayers with an area of about 1 cm^2, whose quality was examined by the laser diffraction experiment (see Supporting Information Section S8). The monolayer orientation or φ_0 could be determined by the diffraction patterns. A 2° fluctuation of φ_0 across the substrate was observed. To obtain Ag nanostructures like those in domain 3, the monocrystalline monolayer was aligned carefully to make $\varphi_0 \approx 50°$ when substrates were mounted in the deposition vacuum chamber. Figure 4d shows the ΔT spectra of Ag films deposited onto the large-area monocrystalline monolayers, as well as the low-quality polycrystalline monolayers, illuminated by the incident light with a beam diameter of 1 cm (see Supporting Information Section S2). The polycrystalline sample was fabricated in counterclockwise substrate rotation as a control and exhibits a

DOI: 10.1021/acsphotonics.5b00196
ACS Photonics 2015, 2, 1246−1252

similar CD response to the previous result.[29] The monocrystalline sample shows a similar CD response to domain 3 due to their similar φ_0, but with a smaller ΔT magnitude, which may result from their small difference in φ_0, the defects, and φ_0 fluctuation in the monocrystalline monolayers. However, the large-area monocrystalline sample still exhibits a large CD signal, which is 1 order of magnitude larger than that of the polycrystalline sample and also much greater than those of the large-area chiral metamaterials reported before.[6,11,28,30,33] In order to develop optical devices for real-world applications, further optimization of the fabrication condition is still needed, such as minimizing the defects in monolayers and tuning the thickness of Ag films.

In conclusion, both morphology and chiroptical response of Ag patchy films on different individual colloid monolayer domains are investigated. A variety of achiral or chiral Ag nanostructures formed on differently oriented monolayer domains show different or even opposite CD responses, originating from their geometric shapes. The relationship between morphological chirality and optical chirality has been clearly revealed. An extremely strong CD response is observed in specific local domains that is 1 order of magnitude larger than the bulk CD. FDTD simulations confirm the CD responses in different monolayer domains and reveal the near-field current distributions at resonances. The contribution of domains with opposite CD responses to the averaged CD signal is also investigated. These Ag patchy films may serve as an excellent biosensor, benefiting from the sharp CD peaks and coexistence of patches with opposite CD responses. Furthermore, the Ag chiral films have been fabricated on the large-area monocrystalline monolayers by carefully choosing the monolayer orientation based on this individual domain study and show the expected CD response. By controlling the monolayer orientation, the CD response can be easily tuned or even reversed. This large-area chiral metamaterial with uniform, strong, and tunable CD response can be potentially developed into optical devices.

■ ASSOCIATED CONTENT

Supporting Information

The Supporting Information is available free of charge on the ACS Publications website at DOI: 10.1021/acsphotonics.5b00196.

Determination of φ_0, spectroscopic microscope, circular polarization conversion, ellipticity spectra, FDTD simulations, optical micrographs of mixtures of domains 7 and 8, T(RCP)/T(LCP) of domain 3, and laser diffraction experiment (PDF)

■ AUTHOR INFORMATION

Corresponding Author

*E-mail: yizhuohe@hal.physast.uga.edu.

Notes

The authors declare no competing financial interest.

■ ACKNOWLEDGMENTS

We gratefully acknowledge support from the National Science Foundation (Grant Nos. ECCS-1029609 and CMMI-1435309).

■ REFERENCES

(1) Valev, V. K.; Baumberg, J. J.; Sibilia, C.; Verbiest, T. Chirality and chiroptical effects in plasmonic nanostructures: fundamentals, recent progress, and outlook. *Adv. Mater.* **2013**, *25*, 2517−2534.

(2) Barron, L. D. *Molecular Light Scattering and Optical Activity*; Cambridge University Press: Cambridge, UK, 2004.

(3) Gansel, J. K.; Thiel, M.; Rill, M. S.; Decker, M.; Bade, K.; Saile, V.; von Freymann, G.; Linden, S.; Wegener, M. Gold helix photonic metamaterial as broadband circular polarizer. *Science* **2009**, *325*, 1513−1515.

(4) Thiel, M.; Rill, M. S.; von Freymann, G.; Wegener, M. Three-Dimensional Bi-Chiral Photonic Crystals. *Adv. Mater.* **2009**, *21*, 4680−4682.

(5) Hentschel, M.; Schaferling, M.; Weiss, T.; Liu, N.; Giessen, H. Three-dimensional chiral plasmonic oligomers. *Nano Lett.* **2012**, *12*, 2542−2547.

(6) Frank, B.; Yin, X. H.; Schaferling, M.; Zhao, J.; Hein, S. M.; Braun, P. V.; Giessen, H. Large-Area 3D Chiral Plasmonic Structures. *ACS Nano* **2013**, *7*, 6321−6329.

(7) Mark, A. G.; Gibbs, J. G.; Lee, T. C.; Fischer, P. Hybrid nanocolloids with programmed three-dimensional shape and material composition. *Nat. Mater.* **2013**, *12*, 802−807.

(8) Yin, X.; Schaferling, M.; Metzger, B.; Giessen, H. Interpreting chiral nanophotonic spectra: the plasmonic Born-Kuhn model. *Nano Lett.* **2013**, *13*, 6238−6243.

(9) Cui, Y.; Kang, L.; Lan, S.; Rodrigues, S.; Cai, W. Giant chiral optical response from a twisted-arc metamaterial. *Nano Lett.* **2014**, *14*, 1021−1025.

(10) Larsen, G. K.; He, Y. Z.; Wang, J.; Zhao, Y. P. Scalable Fabrication of Composite Ti/Ag Plasmonic Helices: Controlling Morphology and Optical Activity by Tailoring Material Properties. *Adv. Opt. Mater.* **2014**, *2*, 245−249.

(11) Ogier, R.; Fang, Y.; Svedendahl, M.; Johansson, P.; Käll, M. Macroscopic Layers of Chiral Plasmonic Nanoparticle Oligomers from Colloidal Lithography. *ACS Photonics* **2014**, *1*, 1074−1081.

(12) Kuzyk, A.; Schreiber, R.; Fan, Z.; Pardatscher, G.; Roller, E. M.; Hogele, A.; Simmel, F. C.; Govorov, A. O.; Liedl, T. DNA-based self-assembly of chiral plasmonic nanostructures with tailored optical response. *Nature* **2012**, *483*, 311−314.

(13) Dietrich, K.; Lehr, D.; Helgert, C.; Tunnermann, A.; Kley, E. B. Circular dichroism from chiral nanomaterial fabricated by on-edge lithography. *Adv. Mater.* **2012**, *24*, OP321−OP325.

(14) Pendry, J. B. A chiral route to negative refraction. *Science* **2004**, *306*, 1353−1355.

(15) Zhang, S.; Park, Y.-S.; Li, J.; Lu, X.; Zhang, W.; Zhang, X. Negative Refractive Index in Chiral Metamaterials. *Phys. Rev. Lett.* **2009**, *102*, 023901.

(16) Zhao, Y.; Belkin, M. A.; Alu, A. Twisted optical metamaterials for planarized ultrathin broadband circular polarizers. *Nat. Commun.* **2012**, *3*, 870.

(17) Turner, M. D.; Saba, M.; Zhang, Q.; Cumming, B. P.; Schröder-Turk, G. E.; Gu, M. Miniature chiral beamsplitter based on gyroid photonic crystals. *Nat. Photonics* **2013**, *7*, 801−805.

(18) Wu, S.; Zhang, Z.; Zhang, Y.; Zhang, K.; Zhou, L.; Zhang, X.; Zhu, Y. Enhanced Rotation of the Polarization of a Light Beam Transmitted through a Silver Film with an Array of Perforated S-Shaped Holes. *Phys. Rev. Lett.* **2013**, *110*, 207401.

(19) Zhang, S.; Zhou, J.; Park, Y. S.; Rho, J.; Singh, R.; Nam, S.; Azad, A. K.; Chen, H. T.; Yin, X.; Taylor, A. J.; Zhang, X. Photoinduced handedness switching in terahertz chiral metamolecules. *Nat. Commun.* **2012**, *3*, 942.

(20) Armelles, G.; Caballero, B.; Prieto, P.; Garcia, F.; Cebollada, A.; Gonzalez, M. U.; Garcia-Martin, A. Magnetic field modulation of chirooptical effects in magnetoplasmonic structures. *Nanoscale* **2014**, *6*, 3737−3741.

(21) Eslami, S.; Gibbs, J. G.; Rechkemmer, Y.; van Slageren, J.; Alarcón-Correa, M.; Lee, T.-C.; Mark, A. G.; Rikken, G. L. J. A.; Fischer, P. Chiral Nanomagnets. *ACS Photonics* **2014**, *1*, 1231−1236.

(22) Kuzyk, A.; Schreiber, R.; Zhang, H.; Govorov, A. O.; Liedl, T.; Liu, N. Reconfigurable 3D plasmonic metamolecules. *Nat. Mater.* **2014**, *13*, 862−866.

(23) Valev, V. K. Characterization of nanostructured plasmonic surfaces with second harmonic generation. *Langmuir* **2012**, *28*, 15454−15471.

DOI: 10.1021/acsphotonics.5b00196
ACS Photonics 2015, 2, 1246−1252

(24) Rodrigues, S. P.; Lan, S.; Kang, L.; Cui, Y.; Cai, W. Nonlinear imaging and spectroscopy of chiral metamaterials. *Adv. Mater.* **2014**, *26*, 6157−6162.
(25) Valev, V. K.; Baumberg, J. J.; De Clercq, B.; Braz, N.; Zheng, X.; Osley, E. J.; Vandendriessche, S.; Hojeij, M.; Blejean, C.; Mertens, J.; Biris, C. G.; Volskiy, V.; Ameloot, M.; Ekinci, Y.; Vandenbosch, G. A.; Warburton, P. A.; Moshchalkov, V. V.; Panoiu, N. C.; Verbiest, T. Nonlinear superchiral meta-surfaces: tuning chirality and disentangling non-reciprocity at the nanoscale. *Adv. Mater.* **2014**, *26*, 4074−4081.
(26) Hendry, E.; Carpy, T.; Johnston, J.; Popland, M.; Mikhaylovskiy, R. V.; Lapthorn, A. J.; Kelly, S. M.; Barron, L. D.; Gadegaard, N.; Kadodwala, M. Ultrasensitive detection and characterization of biomolecules using superchiral fields. *Nat. Nanotechnol.* **2010**, *5*, 783−787.
(27) Larsen, G. K.; He, Y. Z.; Ingram, W.; Zhao, Y. P. Hidden Chirality in Superficially Racemic Patchy Silver Films. *Nano Lett.* **2013**, *13*, 6228−6232.
(28) He, Y.; Larsen, G. K.; Ingram, W.; Zhao, Y. Tunable three-dimensional helically stacked plasmonic layers on nanosphere monolayers. *Nano Lett.* **2014**, *14*, 1976−1981.
(29) Larsen, G. K.; He, Y.; Ingram, W.; LaPaquette, E. T.; Wang, J.; Zhao, Y. The fabrication of three-dimensional plasmonic chiral structures by dynamic shadowing growth. *Nanoscale* **2014**, *6*, 9467−9476.
(30) He, Y.; Larsen, G.; Li, X.; Ingram, W.; Chen, F.; Zhao, Y. Nanoscale Conical Swiss Roll with Broadband Visible and NIR Circular Dichroism. *Adv. Opt. Mater.* **2015**, *3*, 342−346.
(31) Landström, L.; Brodoceanu, D.; Arnold, N.; Piglmayer, K.; Bäuerle, D. Photonic properties of silicon-coated colloidal monolayers. *Appl. Phys. A: Mater. Sci. Process.* **2005**, *81*, 911−913.
(32) Yi, D. K.; Lee, J.-H.; Rogers, J. A.; Paik, U. Two-dimensional nanohybridization of gold nanorods and polystyrene colloids. *Appl. Phys. Lett.* **2009**, *94*, 084104.
(33) Gibbs, J. G.; Mark, A. G.; Eslami, S.; Fischer, P. Plasmonic nanohelix metamaterials with tailorable giant circular dichroism. *Appl. Phys. Lett.* **2013**, *103*, 213101.

DOI: 10.1021/acsphotonics.5b00196
ACS Photonics 2015, 2, 1246−1252